Soft Matter Hot Paper

Superchaotropic Nano-ion Binding as a Gelation Motif in Cellulose Ether Solutions

Max Hohenschutz,* Pierre Bauduin, Carlos G. Lopez, Beate Förster, and Walter Richtering*

Abstract: Nanometer-sized anions (nano-ions) like polyoxometalates and boron clusters exhibit so-called superchaotropic behavior, which describes their strong binding to hydrated non-ionic matter in water. We show here that nano-ions, at millimolar concentrations, dramatically enhance the viscosity and induce gelation of aqueous solutions of non-ionic cellulose ethers (CEs), a class of widely utilized polymers known for their thickening and gel-forming ability. These phenomena arise from an interplay of attractive forces and repulsive electrostatic forces between CE-chains upon nano-ion binding. The attractive forces manifest themselves as aggregation of CE-chains into a physically crosslinked polymer network (gel). In turn, the electrostatic repulsions hamper the viscosity increase and gelation. Superchaotropic nano-ion binding emerges as a novel and general physical crosslinking motif for CE-solutions and exceeds by far the conventional thickening effects of classical salts and ionic surfactants.

Nanometer-sized anions (nano-ions), such as dodecaborates and Keggin polyoxometalates (POMs), have recently emerged as potent inorganic additives for aqueous non-ionic soft matter systems.[1] Their sizes around one nanometer combined with ionic charges typically from −1 to −6, place nano-ions at the boundary between classical ions and charged colloids, which results in fascinating solution properties.[2] In water, due to their very low charge densities, nano-ions are weakly hydrated and exhibit a strong tendency to co-assemble with non-ionic matter.[1b,3] Co-assembly of nano-ions was thus shown to occur with a host of diverse non-ionic solutes including polymers,[4] surfactants,[1a,3b] hydrotropes,[5] and aromatic molecules[6] as well as with interfaces as provided by nanoparticles[2b,7] or non-ionic surfactant-covered water surfaces.[3b,8] The chaotropic effect, an enthalpic, water-mediated driving force that arises from the favorable release of hydration water of the nano-ion and the solute upon contact formation, lies at the bottom of these nano-ion/solute co-assembly phenomena.[3a,9] Nano-ion binding to hydrated organic matter occurs typically in the micro- to millimolar range and may even exceed the binding of classical hydrophobic additives or surfactants.[1a,3a] Since nano-ion/solute co-assembly is much stronger than for classical chaotropic ions, such as SCN^- or I^-, nano-ions were termed superchaotropic ions[3] in extension to the well-known Hofmeister series.[10] Nano-ion co-assembly has thus opened novel pathways to the formulation of hybrid organic/inorganic materials such as foams[8] and inorganic supramolecular networks[11] as well as catalytic[12] and drug delivery[13] applications.

The binding of a nano-ion to a solute typically elicits pronounced changes in the solute's solution behavior. For example, the thermosensitive non-ionic polymer poly n-isopropyl acrylamide (PNiPAM) displays a structural transition from polymer coils to co-assembled $PW_{12}O_{40}^{3-}$/PNiPAM globules and sheets at millimolar concentrations of $PW_{12}O_{40}^{3-}$ accompanied by an increase of 20 K in the lower critical solution temperature (LCST).[4a] These dramatic effects on PNiPAM encouraged us to explore the impact of superchaotropic nano-ions on the solution properties of a group of widely applied non-ionic polymers: cellulose ethers (CEs).

Non-ionic CEs, such as methylcellulose (MC), hydroxyethylcellulose (HEC), or hydroxypropylcellulose (HPC, see Figure 1a) are an important class of water-soluble polymers.[14] Derivatized from wood cellulose, the world's most abundant renewable resource, CEs are available at low cost, and exhibit low toxicity and excellent biocompatibility. Thus, CEs find application in drilling fluids,[15] cosmetics,[16] foods[17] and pharmaceutics[18] due to their viscosifying power[19] in solution, and in superabsorbent materials, as drug carriers in pharmaceutical products and tissue engineering[20] in the form of CE-based hydrogels.[20b,21] The

[*] Dr. M. Hohenschutz, Dr. C. G. Lopez, Prof. W. Richtering
RWTH Aachen University, Institute of Physical Chemistry
Landoltweg 2, 52074 Aachen (Germany)
E-mail: hohenschutz@pc.rwth-aachen.de
richtering@pc.rwth-aachen.de

Dr. P. Bauduin
Institut de Chimie Séparative de Marcoule, ICSM, CEA, CNRS, ENSCM, Univ Montpellier
Marcoule (France)

Dr. B. Förster
Forschungszentrum Jülich GmbH, Ernst Ruska-Centrum für Mikroskopie und Spektroskopie mit Elektronen (ER–C-1)
52425 Jülich (Germany)

Prof. W. Richtering
DWI—Leibniz-Institute for Interactive Materials e.V., RWTH-Aachen University
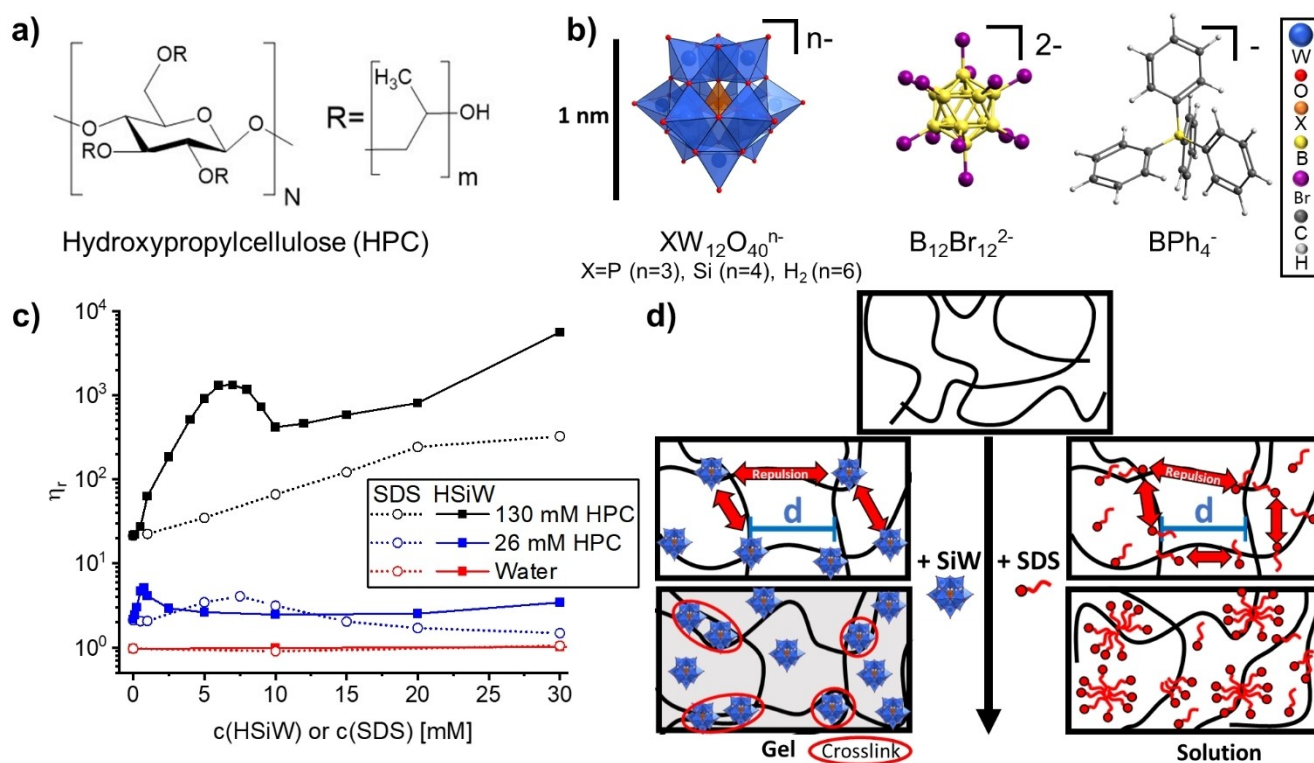Forckenbeckstraße 50, 52074 Aachen (Germany)

Figure 1. a) Chemical structure of HPC. b) Chemical structures of the used nano-ions: Keggin POMs $SiW_{12}O_{40}^{4-}$, $PW_{12}O_{40}^{3-}$, $H_2W_{12}O_{40}^{6-}$, the dodecaborate $B_{12}Br_{12}^{2-}$ and the organic ion BPh_4^-. c) Relative viscosities of HSiW and SDS in water, in HPC-solution at the overlap concentration c*(HPC) = 26 mM and at c(HPC) = 5c* = 130 mM. Lines are guides to the eye. d) Proposed thickening mechanism for SiW compared to the thickening mechanism with SDS gleaned from literature.[24] SDS and HSiW are similar in the initial step of the co-assembly, where SDS or SiW adsorb to the polymer chain causing hydrophobic association of the polymer and inducing electrostatic repulsion (polyelectrolyte behavior). At higher concentrations, SDS and HSiW differ substantially: SDS co-micellizes with the polymer and causes solubilization of the network, while SiW induces crosslinking (red ovals) into a rigid network (gel).

solution viscosities of CEs exceed the ones of synthetic polymers like polyethyleneoxide or polystyrene, owing to the high stiffness of the cellulose backbone and the tendency of hydrophobic patches—due to a heterogeneous degree of substitution (DS) in commercial CEs—along CE-polymers to aggregate.[14b, 22] Gelation of CEs occurs at high concentrations for hydrophobic or low DS samples. Also, at low concentrations, CE-gels can be formed by physical or chemical cross-linking strategies. The former is based on hydrophobic aggregation of CE-chains into a fibrillar network typically above the LCST of the CE,[23] and thus involves heating, while the latter requires synthesis and yields room temperature hydrogels.[20b,21b] Given their significance, fine-tuning of the solution, phase and rheological behavior of CEs is highly desirable.

Herein, we study the effects on solution rheology and structure of the inorganic nano-ion salts $H_4SiW_{12}O_{40}$, $Na_2B_{12}Br_{12}$, $H_3PW_{12}O_{40}$, $(NH_4)_6H_2W_{12}O_{40}$ and the organic nano-ion salt $NaBPh_4$ (all nano-ions shown in Figure 1b) on the non-ionic CEs MC, HEC and HPC. We present the system of HPC with the superchaotropic nano-ion SiW ($SiW_{12}O_{40}^{4-}$, in its acidic form HSiW, $H_4SiW_{12}O_{40}$) as a representative system. Data on the other CE/nano-ion systems are given in the Supporting Information and will be discussed at the end of the paper. The acidic HSiW was used

to ensure pH < 3 in order to avoid decomposition of the plenary α-Keggin POM cluster, which takes place at pH > 4 in water.[25] The used HPC has 3.8 HP units per monomer and a degree of polymerization of N = 230.[26] Concentrations of HPC are expressed as molarity of the monomer throughout the paper.

First, we studied the effects of HSiW on the viscosity of HPC-solutions. Steady shear experiments on HPC in water reveal Newtonian fluid behavior. Upon addition of HSiW, shear thinning arises at high shear rates especially at high HPC- and HSiW-concentrations. The zero-shear viscosities η_0 were extracted from the flow curves as detailed in section S2 and are shown as relative viscosities $\eta_r = \frac{\eta_0}{\eta_{water}}$ in Figure 1c. We find that millimolar concentrations of SiW produce dramatic effects on the viscosity of HPC-solutions. At the overlap concentration c* of HPC (c* ≈ 26 mM ≈ 1% w/w), the viscosity rises four-fold to a maximum at c(HSiW) = 0.75 mM and then decreases. At HSiW-concentrations above 10 mM, a second viscosity increase is observed. For HPC-concentrations above the overlap, c(HPC) = 5c* = 130 mM = 5% w/w, a similar viscosity trend occurs upon HSiW-addition. However, the viscosity increases rapidly by a factor of 100 toward the viscosity maximum at 7 mM HSiW with respect to the HPC-solution without added nano-ion. The magnitude of the viscosity peak decreases

monotonically with HPC-concentration and becomes indiscernible at c*/5, see Figure S2a. As the addition of HSiW has virtually no effect on the viscosity of water, see Figure 1c, HSiW seems to alter HPC-solution viscosity by affecting HPC-HPC interactions.

The effects of HSiW on CE-solution viscosity are reminiscent of the effects of ionic surfactants on non-ionic polymer solutions, which also cause a viscosity maximum.[24] To draw a direct comparison with the effects of HSiW, we measured the viscosity of water and of HPC-solutions at c* and 5c* upon addition of the ionic surfactant sodium dodecylsulfate (SDS, $C_{12}H_{25}SO_4Na$). At $c(HPC) = c* = 26$ mM, SDS-addition also causes a viscosity maximum, see Figure 1c (blue empty symbols). The viscosity maximum is located at $c(SDS) = 7.5$ mM and for $c(SDS) > 15$ mM the viscosity even drops below that of the pure polymer solution. At $c(HPC) = 5c* = 130$ mM, the same trend occurs though the viscosity maximum appears at $c(SDS) = 50$ mM, see Figure S2b. This viscosity trend with SDS-concentration is due to the formation of a pearl necklace structure of SDS-micelles along the polymer above the critical aggregation concentration, shown schematically in Figure 1d.[24] The hydrophobic interaction of the alkyl chain of SDS and the polymer acts as the driving force for the assembly. The viscosity increase is assigned to an interplay of electrostatic repulsion and hydrophobic attraction that arise between polymer chains upon adsorption of SDS. As the polymer becomes saturated with SDS, aggregated chains are solubilized, SDS-micelles form in solution and electrostatics are screened, which causes a subsequent decrease in the solution viscosity.[24b,e] In comparison to SDS, HSiW causes the viscosity peak at much lower concentrations and induces stronger viscosifying effects by nearly two orders of magnitude (Figure 1c dark symbols).

Furthermore, at $c(HPC) = 5c* = 130$ mM and for $c(HSiW) > 30$ mM, rigid gels were formed, see inversion tests[27] in Figure 2a. The transition between viscous solution behavior (downwards flowing) and gel behavior (no flow upon inversion) occurs at 30 mM $< c(HSiW) < 40$ mM. The gels are initially optically clear and become bluish opalescent at $c(HSiW) > 50$ mM and turbid for $c(HSiW) > 100$ mM. The turbid samples are heterogeneous liquid mixtures containing gel-like lumps. In stark contrast, SDS does not induce gelation of HPC as it solubilizes HPC at high SDS-concentrations.[24b,e] Frequency sweeps of viscous HPC/HSiW-solutions and gels allowed for an evaluation of the elastic and energy dissipating properties, see Figure 2b. At 30 mM HSiW, the loss modulus G'' exceeds the storage modulus G', which indicates typical solution behavior. In turn, at 60 mM HSiW, the storage modulus exceeds the loss modulus characteristic for gels. Addition of up to 70 mM HSiW, results in a dramatic increase in the storage modulus with a power law of $G' \propto c^{7.38}$ at 0.1 s^{-1}, see Figure 2c. For $c(HSiW) > 80$ mM, G' deviates from this power law presumably because of the increasing heterogeneity of these samples. The G' of gelled samples, is virtually independent of frequency, see Figure 2b and Figure S16, as expected for well-formed networks. HPC/HSiW-gels therefore behave like an ideal elastic material and G' corresponds to the shear modulus G. Using the theory of rubber elasticity[28] and assuming that all chains participate in the network, we calculated the number of HPC-monomer units between
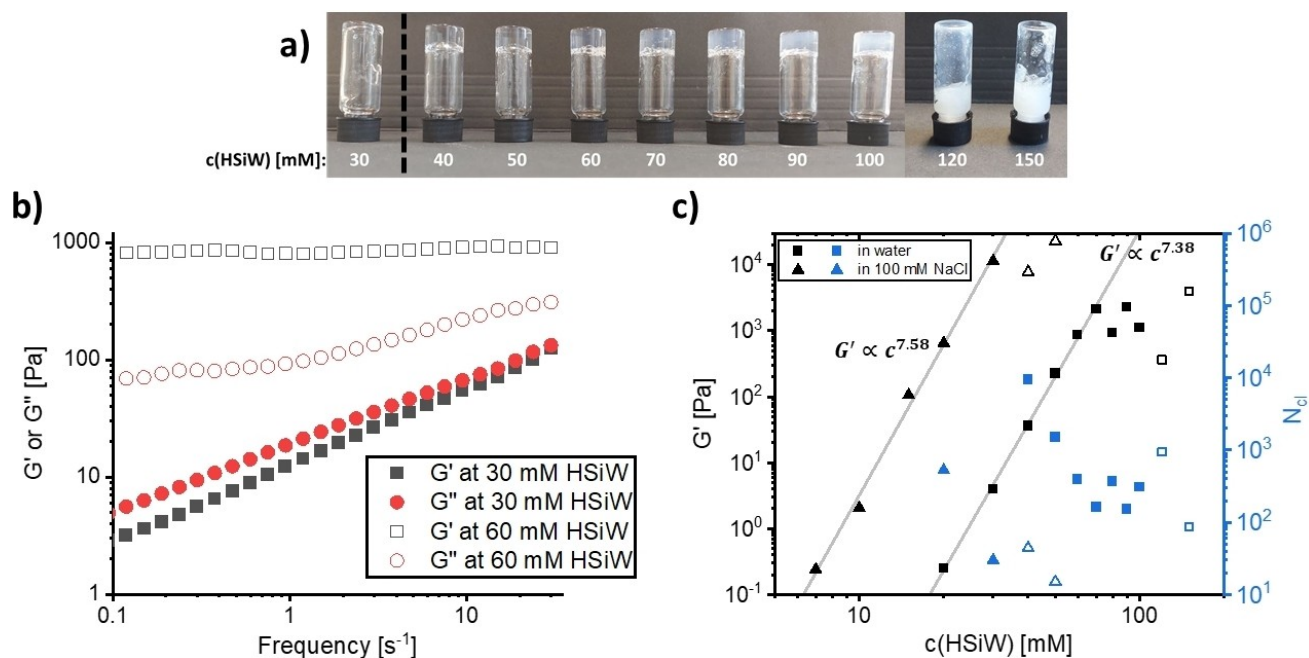

Figure 2. a) Inversion tests of 130 mM HPC with HSiW-concentration. Gels are formed above 30 mM HSiW. Above 100 mM, the samples were turbid and contained gelled lumps b) Frequency sweeps of 130 mM HPC at 30 mM HSiW (solution) and 60 mM HSiW (gel). c) G' at 0.1 s^{-1} and N_{cl}, the number of HPC-monomer units between cross-links, as a function of HSiW-concentration. The grey lines represent power law fits. Empty symbols represent turbid samples.

cross-links $N_{cl} = \frac{k_B Tc}{G}$ with k_B the Boltzmann constant, T the temperature and c the concentration of HPC. Addition of HSiW thus leads to a decrease in N_{cl} from 10^4 to 10^2 (squares in Figure 2c). For the highest G′, considering a cross-link functionality of four, we find 1.3 cross-links per polymer.

We performed equivalent rheological measurements using 100 mM NaCl in water as the solvent and found that gelation is strongly facilitated and ensues already at 10 mM < c(HSiW) < 15 mM, see Figure S17. Correspondingly, the cross-linking effect is enhanced in 100 mM NaCl as shown by much higher G′ and lower values of N_{cl} (triangles in Figure 2c) compared to in water. Up to 7.6 crosslinks per HPC-polymer were formed in 100 mM NaCl by addition of HSiW. The gel strength compared to water increases by a factor of 1000 in 100 mM NaCl as inferred from the differences in G′-values. Notably, the power law exponent in NaCl of $G′ \propto c^{7.58}$ remained close to the one without NaCl ($G′ \propto c^{7.38}$) implying a similar gelation process regardless of the presence of NaCl. In analogy to the enhanced gelling in NaCl, in HPC-solution in 100 mM NaCl the viscosity increases upon HSiW-addition to higher values than in salt-free water, see Figure S3. Since NaCl has no impact on the rheological properties of bare HPC-solutions (Figure S15), NaCl affects the gelation and viscosity of HPC only in the presence of HSiW. By contrast, addition of NaCl to the SDS/HPC-system leads merely to a slight shift of the viscosity peak, see Figure S2b.

In order to elucidate the thickening mechanism of HSiW, we investigate the solution structure in the HPC/HSiW-solutions with Small Angle Neutron Scattering (SANS), Small Angle X-ray Scattering (SAXS) and Cryogenic Transmission Electron Microscopy (Cryo-TEM). Cryo-TEM images show a polymer mesh regardless of the amount of added SiW, see Figure 3a and section S3. The SANS and SAXS measurements further allow for a probing of the system at the nanometer-scale. The SAXS-data are discussed in section S4 as they yielded equivalent insights as SANS-analysis. The SANS profiles of HPC (c = c* = 26 mM) in absence and in the presence of HSiW are shown in Figure 3b. In the SANS-measurements we used D_2O as the solvent instead of H_2O in order to maximize contrast with the hydrogenated HPC, minimize incoherent scattering and to render SiW neutron-transparent. Thus, only the HPC-polymer or the HPC/SiW-assemblies produce scattering, while free SiW-ions cannot be observed.

The SANS-profiles, see Figure 3b, of 26 mM HPC (without HSiW) show a monotonic increase towards low q, which is the typical scattering of semi-rigid polymers. A fit using a cylinder form factor (grey line in Figure 3b, model fitting details in section S10) revealed a cylinder radius of 0.47 nm, corresponding to the expected radius of a single HPC-chain. Thus, HPC-polymers are individually dispersed and non-aggregated. Upon addition of 1 mM HSiW (green triangles), the scattering at high q increases significantly and a correlation peak appears at q* = 0.27 nm⁻¹. The appearance of this correlation peak indicates increased local ordering of the HPC mesh at 1 mM HSiW and corresponds to a mesh size of 23 nm. At q > q*, the intensity scales with a q⁻¹-dependence indicating one-dimensional shape (cylindrical)
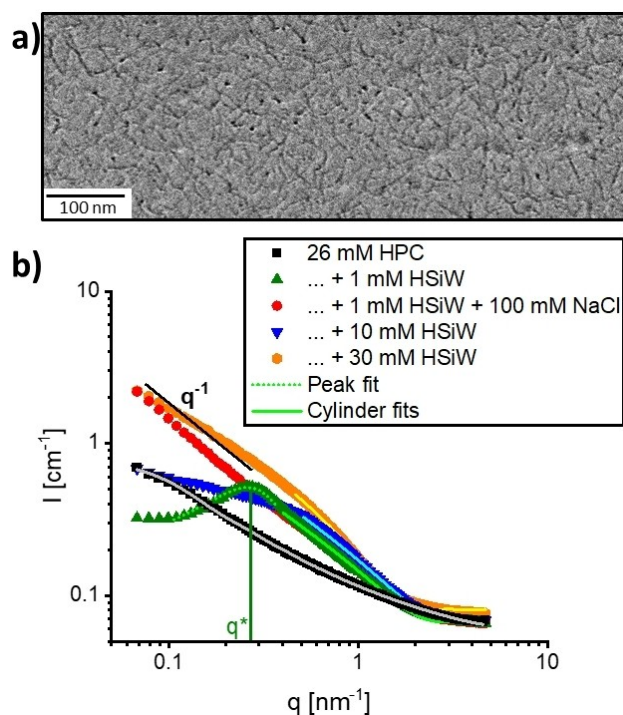

Figure 3. a) Cryo-TEM micrograph of 26 mM HPC + 10 mM HSiW. b) SANS-profiles of 26 mM HPC in bare water and with 1 mM, 10 mM and 30 mM HSiW as well as in the presence of 100 mM NaCl at 1 mM HSiW. Full lines and pointed lines represent form factor and peak fits, respectively. Intensities are in absolute scale. Experimental errors are smaller than the used symbols.

of the scattering object. Fitting with a cylinder form factor in this q-region (solid lines in Figure 3b), resulted in an increased radius of the cylinder of 1.2 nm, which signals SiW-induced aggregation of HPC-chains. Upon further addition of HSiW, the cylinder radius grows to 1.3 nm at 10 mM HSiW and to 1.7 nm at 30 mM HSiW. Additionally, the effect of 100 mM NaCl on the scattering of 26 mM HPC +1 mM HSiW was studied (red circles). The intensity at high q (form factor region) remains unchanged, while the correlation peak disappeared. The disappearance of this correlation peak is gradual with NaCl-addition, see section S4.2, and indicates electrostatic screening. Therefore, adsorbed SiW-ions cause electrostatic repulsions between HPC-chains that become screened upon addition of NaCl. At 1 mM HSiW in water, the HPC/SiW-aggregate can thus be considered as a polyelectrolyte with tetravalent ionic moieties (the charge of SiW is −4) along the chain. A scaling law of $q* \propto c^{0.44}$ (section S4.3) further confirms this polyelectrolyte behavior as it is in good agreement with the theoretical scaling prediction of $q* \propto c^{0.5}$ for semi-dilute polyelectrolytes.[29]

Electrostatic repulsion induced by ion adsorption is a common phenomenon, which is weak for classical chaotropic ions[30] and more pronounced for superchaotropic ions like SiW as shown on non-ionic surfactant self-assemblies (micelles,[1a] bilayers[1a] and foams[8]) as well as PNiPAM-polymer.[4a]

Notably, in Figure 3b, at 10 mM and 30 mM HSiW the correlation peak is absent, presumably due to the presence of excess HSiW that causes a screening effect similar to added NaCl. Consequently, polyelectrolyte behavior of HPC/HSiW occurs only at intermediate HSiW-concentration and affects the viscosity trends shown in Figure 1b in a non-monotonic way. In order to extract a parameter for the strength of the induced electrostatic repulsion, the correlation peak was fitted with a Lorentzian function, which provides an estimate of the peak width, see section S10.1. The sharper the peak, the higher the order in the HPC-network and the stronger is the electrostatic repulsion between chains. A comparison of the peak widths obtained from SAXS and SANS data sets (section S4.4) with the viscosity trends of HSiW reveals that the peaks are the sharpest and thus the electrostatic repulsion (polyelectrolyte behavior) is strongest at the viscosity minimum in Figure 1b, see Figure S11. However, even when the polyelectrolyte behavior is absent, the viscosity increases with HSiW-concentration. Consequently, the viscosity increase must be due to attractive interactions between HPC-chains caused by adsorbed SiW-ions that induce aggregation of HPC-chains into a network structure (gel), as shown schematically in Figure 1d. A similar effect was previously observed for PEO oligomers, where the nano-ion $PW_{12}O_{40}^{3-}$ induced attraction between chains causing precipitation of PEO into a well-defined crystal structure, where each nano-ion is enveloped by two PEO-chains.[31]

^{1}H NMR experiments further enabled to correlate the crosslinking effects with the strength of the interaction of SiW with HPC at the molecular level. The ^{1}H NMR spectra of HPC display a signal of the ether (–CH–O) hydrogens at 3.58 ppm and 3.97 ppm and a singlet at 1.3 ppm of the methyl group (–CH$_3$) in HP, see section S5. These ^{1}H NMR signals shift downfield upon addition of HSiW. The shifts $\Delta\delta$ show saturation behavior at millimolar concentrations, see Figure 4. These shifts are due to the interaction of SiW with the polymer that can be modelled using a Langmuir type equation:[32]

$$\Delta\delta = \frac{\Delta\delta_{max}K_A c}{1 + K_A c}$$

where $\Delta\delta_{max}$ is the maximum shift at saturation in ppm, c the HSiW-concentration in $mol\,L^{-1}$ and K_A the adsorption constant in $L\,mol^{-1}$ denoted as M^{-1}. Fit parameters to the NMR-data are collected in Table S1 in section S5.

We thus observe the highest adsorption constant at the CH$_3$-group ($K_A = 245\,M^{-1}$) indicating the strongest interaction of SiW with CH$_3$ compared to the ether groups with significantly lower K_A-values ($K_A = 187\,M^{-1}$ or $K_A = 197\,M^{-1}$). These differences in binding affinities of SiW reflect slight differences in hydrophobicity of the individual chemical moieties on the polymer. Thus, the CH$_3$-group in HPC is the most hydrophobic one, which enables a slightly tighter binding with the superchaotropic SiW compared to the more hydrophilic ether groups. In comparison, the adsorption of classical chaotropes like SCN$^-$ to non-ionic polymers (PEO, PNiPAM) features adsorption constants typically between 1 and $10\,M^{-1}$.[32b,33] The adsorption constants of SiW with HPC, as shown herein, are 20 times as high, which illustrates a much stronger interaction for SiW than for classical chaotropes. This high adsorption constant underpins the superchaotropic nature of SiW and its high affinity towards neutral soft matter. Interestingly, recent supramolecular binding studies of SiW to γ-cyclodextrin (CD) yield binding constants in the order of $10\,000\,M^{-1}$,[9] 50 times as high as for HPC determined here. As both HPC and γ-CD consist of repeating glucose units and are thus chemically similar, this large difference in binding affinity seems to arise from the differing geometry of the binding site in the host molecules as topography (local curvature) affects the hydrophobicity of the host interface.[32b,34] For γ-CD, the concave cavity is known to be hydrophobic and contain "high energy water",[35] which is released favorably into the bulk upon binding. Thus, γ-CD binds SiW more tightly than HPC, around which hydration water is not subjected to geometric constraints. Additionally, the binding sites in HPC are rather undefined, while in γ-CD the well-defined cavity allows for a good size-match[9] with SiW further facilitating binding. Notably, binding affinities to γ-CD and functionalized Hydroxypropγl-CD (the macrocyclic equivalent to HPC) are expected to be similar,[36] which points at the insignificance of chemical differences between HPC and γ-CD for the binding in comparison to their topographical differences.

We further found that upon adsorption of SiW to HPC, a fraction of H$^+$-counterions (up to 1 H$^+$ per 2 SiW) might co-adsorb as shown by pH-measurements, see section S6.

The other superchaotropic ions $PW_{12}O_{40}^{3-}$, $B_{12}Br_{12}^{2-}$ and BPh_4^- also produced viscosity peaks (all below 10 mM), see section S7, and induced the gelation of HPC solutions, see section S8.1. In comparison, the classical salts NaCl and NaSCN (weakly chaotropic due to the high charge density of the anions compared to superchaotropes) did not produce any effects on HPC solution viscosity (section S7) owing to
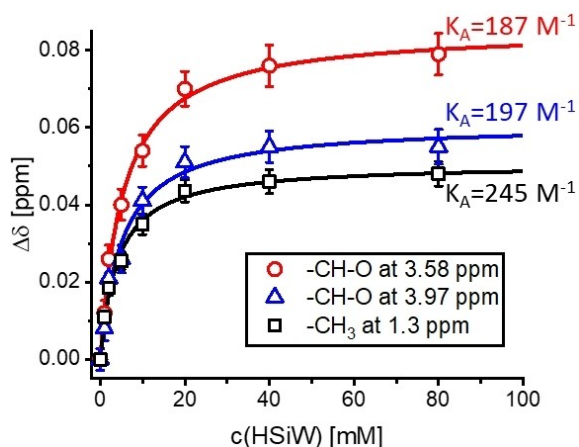
Figure 4. ^{1}H NMR shifts of the three main HPC-signals as a function of HSiW-concentration. The lines indicate Langmuir model fits (all with $R^2 > 0.985$) that yield the adsorption constants K_A. The error bars represent an error propagation of reading uncertainties in the peak positions.

their low binding affinity to non-ionic matter.[3b] Furthermore, methylcellulose and hydroxyethylcellulose solutions formed gels upon addition of the superchaotropic nano-ions $SiW_{12}O_{40}^{4-}$ and $PW_{12}O_{40}^{3-}$, respectively, see section S8.2. The viscosifying and gelation mechanism can therefore be generalized to other superchaotropic ions as well as CEs. The concentration range needed to viscosify or gel a CE-solution, in turn depends on the CE/nano-ion pair, see section S9. Among the tested nano-ions, $PW_{12}O_{40}^{3-}$ emerged as the strongest gelling agent followed by $SiW_{12}O_{40}^{4-}$, BPh_4^- and $B_{12}Br_{12}^{2-}$. By contrast, the Keggin POM $H_2W_{12}O_{40}^{6-}$, a weakly chaotropic nano-ion,[9] did not induce any effects on viscosity (section S7) or structure (section S4.1) of HPC-solutions in line with its weak binding to γ-CD.

In conclusion, we demonstrate that the interaction of superchaotropic nano-ions with non-ionic CEs is a universal phenomenon that leads to a dramatic thickening—much stronger than for classical salts and ionic surfactants—of CE-solutions into gels. The adsorption of the nano-ion to the CE occurs at millimolar concentrations and causes an interplay of attractive and repulsive forces between CE-chains. The attractions arise because the nano-ion minimizes its contact area with water by surrounding itself with CE-chains, which leads to chain aggregation and crosslinking into a polymer network (gel), see Figure 1d. However, repulsive forces (polyelectrolyte behavior) arise at intermediate nano-ion concentrations, where adsorbed nano-ions repel electrostatically. Thus, CE-chains become repulsive, which hampers their aggregation and correlates with a decrease in solution viscosity. When the repulsive electrostatics are screened by addition of electrolyte or excess nano-ion, the thickening effect of the nano-ion is enhanced, and gelation of the CE is facilitated.

The physical crosslinking of CEs at room temperature into optically clear hydrogels by superchaotropic nano-ions provides a novel and facile alternative to conventional heat-induced physical and chemical crosslinking strategies. The crosslinking of neutral polymers by simple addition of superchaotropic nano-ions extends the "physical cross-linking toolbox" for the formation of macromolecular networks, which commonly involves electrostatic approaches such as ion bridging with multivalent ions (also nano-ions[37]), hydrogen bonding or hydrophobic interactions. Since superchaotropic nano-ions span from POMs, which have interesting and tunable catalytic[38] and electronic[39] properties, to the toxicologically benign dodecaborates[13,40] with uses in pharmaceutics,[40a] we expect nano-ion/CE-hydrogels and solutions to be promising candidates for novel hybrid smart materials that exploit synergisms between the nano-ion and the CE.

Acknowledgements

Conflict of Interest

The authors declare no conflict of interest.

Data Availability Statement

The data that support the findings of this study are available from the corresponding author upon reasonable request.

[1] a) M. Hohenschutz, I. Grillo, O. Diat, P. Bauduin, *Angew. Chem. Int. Ed.* **2020**, *59*, 8084–8088; *Angew. Chem.* **2020**, *132*, 8161–8165; b) K. I. Assaf, W. M. Nau, *Angew. Chem. Int. Ed.* **2018**, *57*, 13968–13981; *Angew. Chem.* **2018**, *130*, 14164–14177.

[2] a) A. Malinenko, A. Jonchère, L. Girard, S. Parrès-Maynadié, O. Diat, P. Bauduin, *Langmuir* **2018**, *34*, 2026–2038; b) C. Drummond, L. Pérez-Fuentes, D. Bastos-González, *J. Phys. Chem. C* **2019**, *123*, 28744–28752; c) T. Liu, *Langmuir* **2010**, *26*, 9202–9213.

[3] a) K. I. Assaf, M. S. Ural, F. Pan, T. Georgiev, S. Simova, K. Rissanen, D. Gabel, W. M. Nau, *Angew. Chem. Int. Ed.* **2015**, *54*, 6852–6856; *Angew. Chem.* **2015**, *127*, 6956–6960; b) B. Naskar, O. Diat, V. Nardello-Rataj, P. Bauduin, *J. Phys. Chem. C* **2015**, *119*, 20985–20992.

[4] a) T. Buchecker, P. Schmid, I. Grillo, S. Prévost, M. Drechsler, O. Diat, A. Pfitzner, P. Bauduin, *J. Am. Chem. Soc.* **2019**, *141*, 6890–6899; b) P. Schmid, X. Graß, P. Bahadur, I. Grillo, O. Diat, A. Pfitzner, P. Bauduin, *Colloids Interfaces* **2022**, *6*, 16.

[5] a) P. Schmid, T. Buchecker, A. Khoshsima, D. Touraud, O. Diat, W. Kunz, A. Pfitzner, P. Bauduin, *J. Colloid Interface Sci.* **2021**, *587*, 347–357; b) P. Schmid, M. Hohenschutz, X. Graß, M. Witzmann, D. Touraud, O. Diat, A. Pfitzner, P. Bauduin, *J. Mol. Liq.* **2022**, *359*, 119214.

[6] J. Luo, K. Chen, P. Yin, T. Li, G. Wan, J. Zhang, S. Ye, X. Bi, Y. Pang, Y. Wei, T. Liu, *Angew. Chem. Int. Ed.* **2018**, *57*, 4067–4072; *Angew. Chem.* **2018**, *130*, 4131–4136.

[7] D. Bastos-González, L. Perez-Fuentes, C. Drummond, J. Faraudo, *Curr. Opin. Colloid Interface Sci.* **2016**, *23*, 19–28.

[8] M. Hohenschutz, I. Grillo, C. Dewhurst, P. Schmid, L. Girard, A. Jonchère, O. Diat, P. Bauduin, *J. Colloid Interface Sci.* **2021**, *603*, 141–147.

[9] S. Yao, C. Falaise, A. A. Ivanov, N. Leclerc, M. Hohenschutz, M. Haouas, D. Landy, M. A. Shestopalov, P. Bauduin, E. Cadot, *Inorg. Chem. Front.* **2021**, *8*, 12–25.

[10] a) W. Kunz, *Specific ion effects*, World Scientific, **2010**; b) F. Hofmeister, *Arch. Exp. Path. Pharm.* **1888**, *24*, 247–260.

[11] a) W. Wang, X. Wang, J. Cao, J. Liu, B. Qi, X. Zhou, S. Zhang, D. Gabel, W. M. Nau, K. I. Assaf, *Chem. Comm.* **2018**, *54*, 2098–2101; b) S. Khlifi, J. Marrot, M. Haouas, W. E. Shepard, C. Falaise, E. Cadot, *J. Am. Chem. Soc.* **2022**, *144*, 4469–4477.

[12] P. Schmid, G. Jost, X. Graß, D. Touraud, O. Diat, A. Pfitzner, P. Bauduin, *Green Chem.* **2022**, *24*, 2516–2526.

[13] A. Barba-Bon, G. Salluce, I. Lostalé-Seijo, K. Assaf, A. Hennig, J. Montenegro, W. M. Nau, *Nature* **2022**, *603*, 637–642.

[14] a) D. Klemm, B. Heublein, H. P. Fink, A. Bohn, *Angew. Chem. Int. Ed.* **2005**, *44*, 3358–3393; *Angew. Chem.* **2005**, *117*, 3422–3458; b) W. Burchard, *Cellulose* **2003**, *10*, 213–225.

[15] K. Liu, H. Du, T. Zheng, H. Liu, M. Zhang, R. Zhang, H. Li, H. Xie, X. Zhang, M. Ma, *Carbohydr. Polym.* **2021**, *259*, 117740.

[16] H. Ullah, H. A. Santos, T. Khan, *Cellulose* **2016**, *23*, 2291–2314.

[17] X. He, W. Lu, C. Sun, H. Khalesi, A. Mata, R. Andaleeb, Y. Fang, *Carbohydr. Polym.* **2021**, *255*, 117334.

[18] H. C. Arca, L. I. Mosquera-Giraldo, V. Bi, D. Xu, L. S. Taylor, K. J. Edgar, *Biomacromolecules* **2018**, *19*, 2351–2376.

[19] C. Clasen, W. M. Kulicke, *Prog. Polym. Sci.* **2001**, *26*, 1839–1919.

[20] a) H. Du, W. Liu, M. Zhang, C. Si, X. Zhang, B. Li, *Carbohydr. Polym.* **2019**, *209*, 130–144; b) C. Chang, L. Zhang, *Carbohydr. Polym.* **2011**, *84*, 40–53.

[21] a) A. Sannino, C. Demitri, M. Madaghiele, *Materials* **2009**, *2*, 353–373; b) E. Ruel-Gariépy, J.-C. Leroux, *Eur. J. Pharm. Biopharm.* **2004**, *58*, 409–426; c) M. Vázquez-González, I. Willner, *Angew. Chem. Int. Ed.* **2020**, *59*, 15342–15377; *Angew. Chem.* **2020**, *132*, 15458–15496.

[22] a) B. Lindman, B. Medronho, L. Alves, C. Costa, H. Edlund, M. Norgren, *Phys. Chem. Chem. Phys.* **2017**, *19*, 23704–23718; b) C. G. Lopez, R. H. Colby, J. T. Cabral, *Macromolecules* **2018**, *51*, 3165–3175.

[23] a) L. Li, *Macromolecules* **2002**, *35*, 5990–5998; b) N. Sarkar, *J. Appl. Polym. Sci.* **1979**, *24*, 1073–1087; c) C. Carotenuto, N. Grizzuti, *Rheol. Acta* **2006**, *45*, 468–473.

[24] a) E. D. Goddard, *Colloids Surf.* **1986**, *19*, 255–300; b) S. John Bosco, H. Zettl, J. J. Crassous, M. Ballauff, G. Krausch, *Macromolecules* **2006**, *39*, 8793–8798; c) S. Nilsson, *Macromolecules* **1995**, *28*, 7837–7844; d) C. J. Drummond, S. Albers, D. N. Furlong, *Colloids Surf.* **1992**, *62*, 75–85; e) S. M. C. Silva, F. E. Antunes, J. J. S. Sousa, A. J. M. Valente, A. A. C. C. Pais, *Carbohydr. Polym.* **2011**, *86*, 35–44.

[25] a) A. Jürgensen, J. B. Moffat, *Catal. Lett.* **1995**, *34*, 237–244; b) B. J. Smith, V. A. Patrick, *Aust. J. Chem.* **2002**, *55*, 281–286; c) D. Bajuk-Bogdanović, S. Uskoković-Marković, I. Holclajtner-Antunović, *J. Iran. Chem. Soc.* **2015**, *12*, 137–145.

[26] C. G. Lopez, L. Voleske, W. Richtering, *Carbohydr. Polym.* **2020**, *234*, 115886.

[27] R. D. Sydansk, *SPE Reservoir Eng.* **1990**, *5*, 346–352.

[28] M. Rubinstein, R. H. Colby, *Polymer physics, Vol. 23*, Oxford university press New York, **2003**.

[29] A. V. Dobrynin, R. H. Colby, M. Rubinstein, *Macromolecules* **1995**, *28*, 1859–1871.

[30] E. Leontidis, *Curr. Opin. Colloid Interface Sci.* **2002**, *7*, 81–91.

[31] T. Buchecker, X. Le Goff, B. Naskar, A. Pfitzner, O. Diat, P. Bauduin, *Chem. Eur. J.* **2017**, *23*, 8434–8442.

[32] a) K. B. Rembert, J. Paterová, J. Heyda, C. Hilty, P. Jungwirth, P. S. Cremer, *J. Am. Chem. Soc.* **2012**, *134*, 10039–10046; b) B. A. Rogers, H. I. Okur, C. Yan, T. Yang, J. Heyda, P. S. Cremer, *Nat. Chem.* **2022**, *14*, 40–45.

[33] Y. Zhang, S. Furyk, D. E. Bergbreiter, P. S. Cremer, *J. Am. Chem. Soc.* **2005**, *127*, 14505–14510.

[34] a) R. Godawat, S. N. Jamadagni, S. Garde, *Proc. Natl. Acad. Sci. USA* **2009**, *106*, 15119–15124; b) E. Xi, V. Venkateshwaran, L. Li, N. Rego, A. J. Patel, S. Garde, *Proc. Natl. Acad. Sci. USA* **2017**, *114*, 13345–13350; c) Y.-K. Cheng, P. J. Rossky, *Nature* **1998**, *392*, 696–699.

[35] F. Biedermann, W. M. Nau, H. J. Schneider, *Angew. Chem. Int. Ed.* **2014**, *53*, 11158–11171; *Angew. Chem.* **2014**, *126*, 11338–11352.

[36] S. E. Hollow, T. C. Johnstone, *Chem. Comm.* **2022**, *58*, 2375–2378.

[37] a) J. Li, R. Fernandez-Alvarez, Z. Tošner, S. Kereïche, M. Uchman, P. Matějíček, *J. Mol. Liq.* **2021**, *336*, 116367; b) H. Wei, N. Shi, J. Zhang, Y. Guan, J. Zhang, X. Wan, *Chem. Comm.* **2014**, *50*, 9333–9335.

[38] a) S.-S. Wang, G.-Y. Yang, *Chem. Rev.* **2015**, *115*, 4893–4962; b) M. T. Pope, A. Müller, *Angew. Chem. Int. Ed. Engl.* **1991**, *30*, 34–48; *Angew. Chem.* **1991**, *103*, 56–70.

[39] Y.-F. Song, R. Tsunashima, *Chem. Soc. Rev.* **2012**, *41*, 7384–7402.

[40] a) E. Hey-Hawkins, C. V. Teixidor, *Boron-based compounds: potential and emerging applications in medicine*, John Wiley & Sons, Hoboken, **2018**; b) K. Fink, M. Uchman, *Coord. Chem. Rev.* **2021**, *431*, 213684.